Journal of Nanophotonics, 9(1) (2015) 093067

Multi-Exposure Laser Interference Lithography

Abdollah Hassanzadeh,[a*] Mohammadbagher Mohammadnezhad[a] and Silvia Mittler[b]
[a]University of Kurdistan, Faculty of Sciences, Department of Physics, Pasdaran Street, Sanandaj, Iran, 66177-15177
[b]University of Western Ontario, Department of Physics and Astronomy, London, ON, N6A 3K7, Canada

Abstract. Nanopatterns resulting from two beam interference in single, double and multi-exposures were simulated. Several patterns were fabricated for comparison of experiment and simulation allowing to judge the qulity of the simulation tool. Experimental and simulation results were consistent for single and double exposures. Photoresist nanofibers attached and detached from the substrate were fabricated with little changes in the development procedure. It is shown that with increasing number of exposures a wide variety of patterns with very fine structures and sophisticated geometries can be generated. Fresnel-lens type structures are formed when the number of exposures was increased. These may find applications in areas such as security patterns and diffractive optical elements.

Keywords: nanostructures, interference lithography, photoresist, periodic structures.

Address all correspondence to: Abdollah Hassanzadeh, University of Kurdistan, Faculty of Sciences, Department of Physics, Pasdaran street, Sanandaj, Iran, Postal Code: 66177-15175, Tel: +98 8733664600, Fax: +98 87-3366-0075, E-mail: A.Hassanzadeh@uok.ac.ir

1 Introduction

Periodic micro- and nanostructures have found numerous applications in different optical fields such as antireflection coating layers,[1] photonic crystals,[2] diffraction gratings,[3] magnetic devices,[4] biochemical sensors and surface optics,[5] diffractive lenses,[6] but also in biology, such as the assessment of the adhesion and expansion of periodontal ligament (PDL) fibroblasts.[7]

There are several techniques for fabricating nanostructures on solid substrates, such as ion beam lithography (IBL) or electron beam lithography (EBL). These methods have advantages in the fabrication of structures at scales smaller than optical lithography with flexibility in the pattern design. However, they are time-consuming, involving multistep procedures, are expensive and not able to produce nanostructures on large areas (many square centimeters).[1, 4]

An alternative method for the fabrication of nanopatterns on solid substrates is laser interference lithography (LIL) where two or more coherent laser beams interfere on a substrate covered with a layer of photoresist.[8, 9] This lithographic technique relies on constructive and destructive interference writing pattern into photoresist films. LIL is a fast and inexpensive, mask-less technique which can be used to fabricate periodic defect free nanostructures with exceptional pattern flexibility over large areas.

A variety of 1D, 2D and 3D nano- and microstructures such as membrane reflectors,[10] microsieves,[11] guided-wave gratings,[12, 13] periodic magnetic nanodot arrays,[4] microdisks,[14] photonic crystals for the visible spectrum,[15] three-dimensional periodic patterns,[16] 3-D polymeric photonic structures,[17] recording holographic micropatterns in film systems,[18] have been fabricated using multi-beam laser interference and multiple exposure lithography.

We doubt that LIL's potential abilities have been fully revealed yet. To show several additional capabilities of LIL, we present simulations and experimental results of single and multiple exposure samples. The interference patterns obtained from simulations for multiple exposures (e.g. 6 successive exposures) show a wide variety of structures. As an example, Fresnel-lense[19] type structures appear when the number of exposures is increased.

2 Two beam interference

There are various configurations for LIL. However, the Lloyd's mirror configuration is the most used arrangement among them.[20] The Lloyd's mirror interferometer is based on the interference of two coherent laser beams. It consists of a mirror which is usually mounted perpendicular to the sample carrying the photoresists. It is worth to mention that new configurations for Lloyd's mirror interferometer have been introduced mounting the mirror in a non-perpendicular fashion

to the sample.[10, 12] For all configurations of the Lloyd's mirror interferometer a laser beam is incident on both the mirror and the sample. The portion of the beam which is reflected off the mirror surface interferes with the part of the beam that is directly incident on the sample (Fig.1a). This interference leads to an intensity distribution in the photoresist (Fig. 1(b)) where, after the resist's developing, parallel photoresist stripes on the sample surface are present. Mesh-like patterns can be obtained using a double-exposure technique, where after the first exposure the substrate is rotated by 90° and is exposed again.[11-13, 21-23]

One of the principal advantages of the Lloyd's mirror technique is its simplicity to create a variety of low cost periodic nanoscale patterns over a relatively large substrate area with high throughput.[5, 20, 23-25]

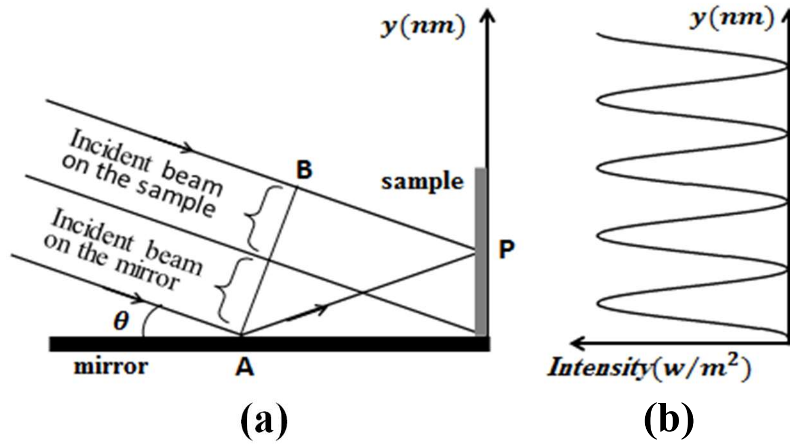

Fig. 1 Schematic diagram of the Lloyd's mirror interferometer: (a) basic experimental set-up, (b) intensity distribution on the sample in the case of a homogeneous intensity profile in the laser beam.

3. Theoretical Background

We consider interference between two linearly polarized plane waves of the forms

$$\vec{E}_1(\vec{r},t) = \vec{E}_{01}\cos(\vec{k}_1.\vec{r} - \omega t + \varepsilon_1), \quad (1)$$

$$\vec{E}_2(\vec{r},t) = \vec{E}_{02}\cos(\vec{k}_2.\vec{r} - \omega t + \varepsilon_2), \quad (2)$$

where $\vec{E}_1(\vec{r},t)$ and $\vec{E}_2(\vec{r},t)$ represent electric fields of interfering waves, at the observation point P, defined by position vector $\vec{r}$, in time t, and $\vec{E}_{01}$and $\vec{E}_{02}$ are two wave amplitudes, $\vec{k}_1$ and $\vec{k}_2$ are propagation vector of two waves, ε_1 and ε_2 are initial phase angles, Both waves have the same frequency ω. Based on the principle of superposition ($\vec{E} = \vec{E}_1 + \vec{E}_2$) and relation between amplitude of an electromagnetic wave with its irradiance ($I = c\varepsilon_0 E_0^2/2$) the following can be obtained for the total irradiance of the two interfering waves on the sample

$$I = I_1 + I_2 + I_{12}, \tag{3}$$

where I_1 and I_2 are irradiances of the individual waves, I_{12} is known as the interference term which interference term given by

$$I_{12} = \vec{E}_{01}.\vec{E}_{02}\cos\delta, \tag{4}$$

With δ representing the phase difference resulting from path length differences and the initial phase differences. It can be expressed by

$$\delta = (\vec{k}_2 - \vec{k}_1).\vec{r} + (\varepsilon_2 - \varepsilon_1), \tag{5}$$

In the case where the electric fields of incoming waves $\vec{E}_{01}$ and $\vec{E}_{02}$ are polarized and parallel, the interference term can be simplified and written as

$$I_{12} = 2\sqrt{I_1 I_2}\cos(\delta), \tag{6}$$

Where in addition both interfering beams have equal amplitudes ($I_1 = I_2 = I_0$) Eq. (6) leads to

$$I = 4I_0 cos^2(\delta/2), \tag{7}$$

Equation (7) is used here to obtain the interference intensity pattern of a Lloyd's mirror interferometer. According to Fig.1 and taking an additional phase shift of π for the reflection from the mirror surface into account, the following equation for δ can be obtained

$$\delta = (2\pi/\lambda) \times (2y\sin\theta) + \pi, \tag{8}$$

where λ is the incident beam wavelength, y is the component of the $\vec{r}$ vector at point P on the sample, and θ is the angle between the mirror surface and the incident beam. The first term represents the phase difference resulting from the path length difference $|AP - BP|$ (Fig.1). By substituting Eq. (8) into Eq. (7) the intensity distribution in the photoresist is obtained

$$I = 4I_0 sin^2(2\pi y \, sin\,\theta/\lambda), \tag{9}$$

According to Eq. (9), the periodicity of the fringes is obtained by

$$P = \lambda/2\,sin\,\theta, \tag{10}$$

It can be seen from Eq. (10) that P increases with increasing λ and when the incident angle θ increase from 0 to $\pi/2$, P decreases from infinity to $\lambda/2$.

4 Experimental

Fig.2 shows the scheme of the Lloyd's mirror interference lithography setup. It consists of a high reflectivity mirror and a sample holder which is mounted perpendicularly to the mirror on a rotation stage. Positive photoresist S 1805 (Shipley) was spin-coated at 3000 rpm for 45 seconds onto the glass substrates. The photoresist is diluted by the thinner P to reach the desired thickness around several hundreds of nanometers. Prior to exposure the photoresist is soft-baked for 30 minutes at 90 °C. A continuous laser wave emitted from a HeCd laser at $\lambda = 442\,nm$ was focused by a 40x objective lens into a pinhole with a diameter of $5\mu m$. The beam then was collimated by a lens with f = 20cm. After exposure, the photoresist was developed in M319 developer and hard baked at 120 °C for 30 minutes. The fabricated structures were characterized by SEM.

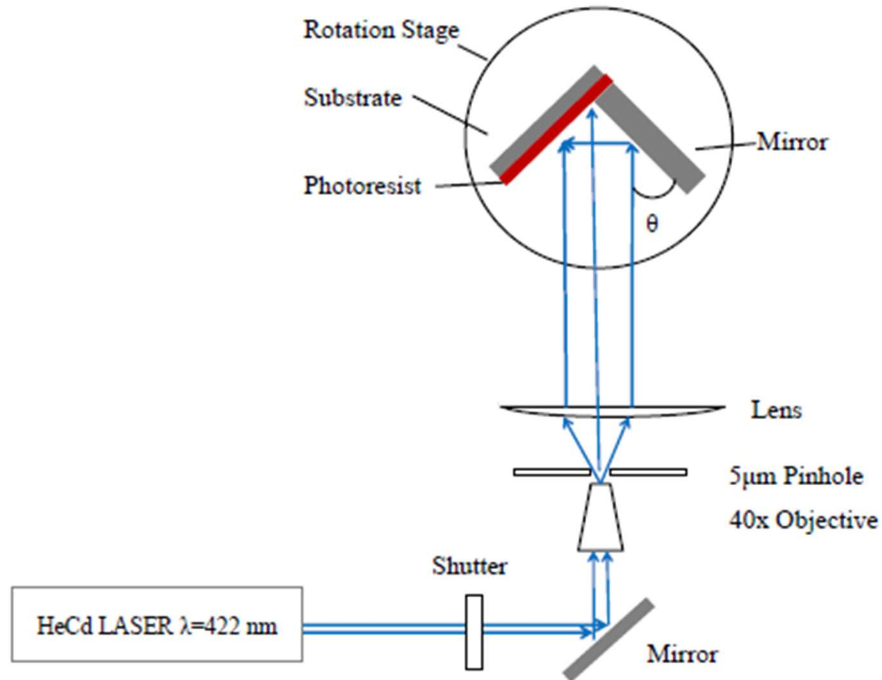

Fig.2 Configuration of the employed LIL setup.

5 Results

In order to test our simulation software and to test photoresist nanofiber production we have fabricated single and double exposed structures similar to the previously demonstrated structures by Ertorer et al.[23]. Fig. 3a shows an electron microscopy image of a single exposure sample, Fig. 3b of the corresponding simulation: parallel stripes. For $\lambda = 442\ nm$ and $\theta = 19.8^{\circ}$ it leads to nanopatterns with periodicity of $652\ nm$. The obtained experimental data are in excellent agreement with the simulations.

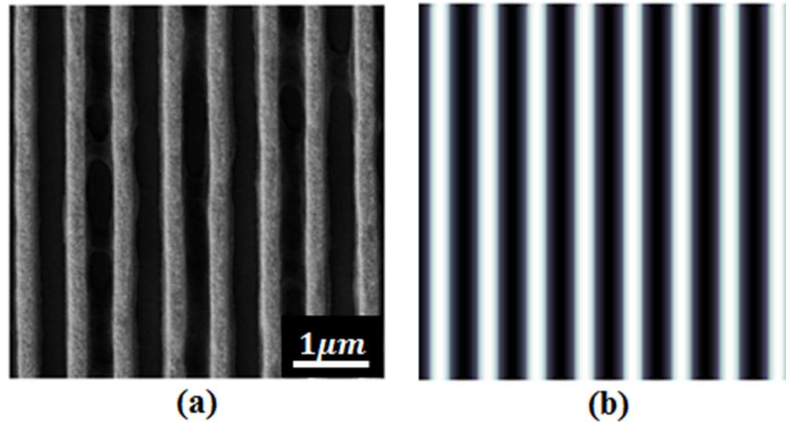

Fig. 3 Interference pattern from a single exposure: (a) SEM image of a LIL fabricated photoresist sample, and (b) simulation results. The angle between the mirror and the sample in the LIL setup was 20˚.

Fabricating nanofibers (Fig.4) on solid substrates and detaching nanofibers are possible with LIL. To create nanofibers the sample needs to be developed carefully. The nanofiber samples were exposed once to achieve the stripe pattern. Development time was increased by 5 seconds. Increasing the development time further detaches the photoresist nanofibers from the substrate. A diameter of 200 nm was achieved for the shown photoresist nanofibers (Fig.4).

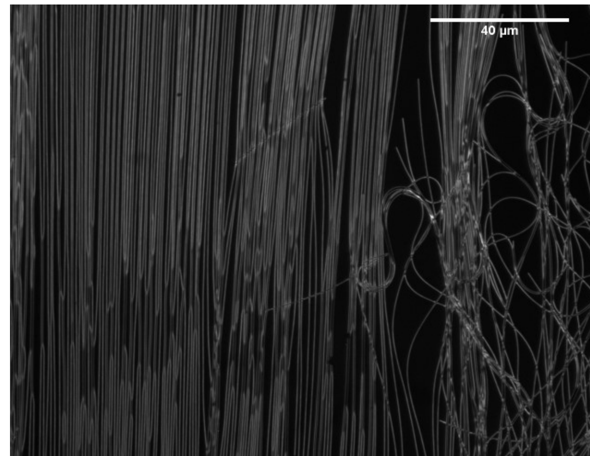

Fig. 4 Micrograph of photoresist nanofibers on a silicon wafer. The diameter of the nanofibers is 200 nm.

In LIL-double-exposure experiments the sample is rotated by an angle 90° after the first exposure. Fig. 4(a) to 4(d), show simulation and experimental results for LIL-double-exposure with different (4(a) and 4(b)) and equal (4(c) and 4(d)) expousr times. Again an excellent

agreement between experiment and simulation can be seen. We conclude: by achieving an excellent agreement between experiment and theory also in comparison to[26] that our simulation software produces reliable results.

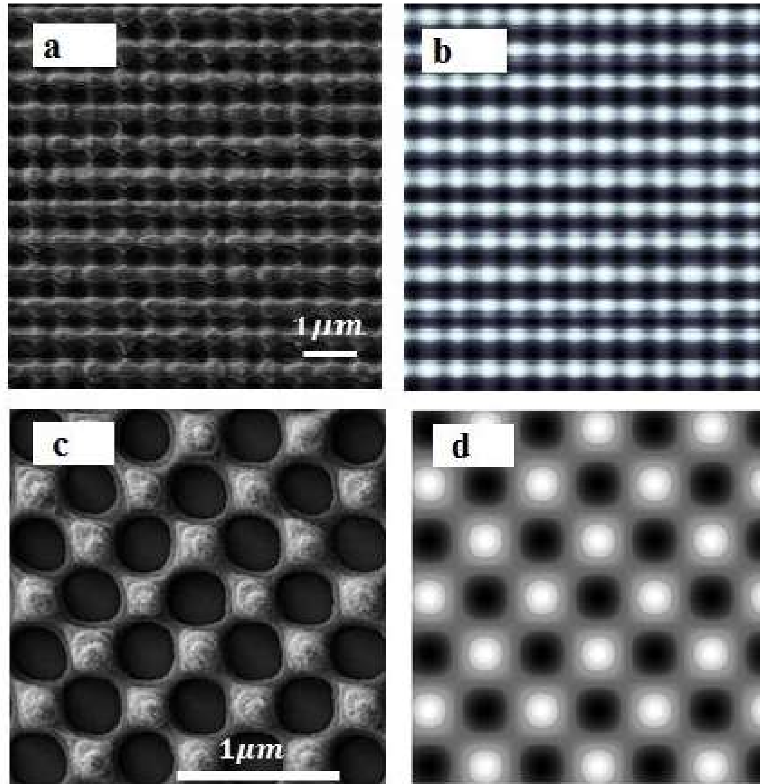

Fig. 5 Example from a double exposure: (a and c) SEM image of the photoresist pattern, and (b and d) simulation results. The exposure times for the first and the second exposures are t_1=30 s and $t_2 = 20$ s for (a and b) and, are t_1=30 s and $t_2 = 30$ s for (c and d), respectively.

The obtained results here and in[26] show that with increasing the number of exposures and varying exposure times, a wide variety of patterns with very fine structures and sophisticated geometries, presenting high order symmetry, can be created. These structures can improve the adhesion or wetting properties, induce random lashing and enhance the light output in emitting devices or can be used in cell adhesion studies.[9, 23, 27-30]

Potential applications of nanostructures can be predicted when information on their dimensions and shapes are available. Obtaining such information experimentally is expensive and time

consuming. However simulation is helpful, quick and cost effective. Letailleur et al. have reported 5-6 exposure experimental results which are in good agreement with simulated interference patterns.[9] To further study the possibilities we have simulated LIL experiments with multiple exposures. In multiple LIL-exposure experiments the sample is exposed n-times with n individual exposure times and rotated in-between by $360°/n$. We use the index i to label the successive exposures. t_i and ϕ_i represent the exposure time and rotation angle corresponding to exposure number i, respectively. However, not neccesarely the rotation angles and the exposre times have to be chosen all identical, respectively. A huge variation spectrum is available. Four different simulated interference patterns are presented in Fig. 6 for n exposures with n = 3, 4, 12 and 36. Here all exposure times were chosen equal as well as the rotation angle ($\phi_i = \phi_{i+1}$ and $t_i = t_{i+1}$). Fig. 6(a) at n = 3 shows a hexagonal pattern of homogeneously distributed dots. Fig. 6b consists of sophisticated shapes which are distributed around dots. These dots form an octagonal pattern as clarified by the lines in the center of the image. We see that 2n is the symmetry order for each pattern which is reasonable having the mirror assembly of the Lloyd interferometer in mind. Fig.6b to 6d show that when the number of exposures exceeds three ($n > 3$), circular patterns appear at the central part of the sample, right there where the center of rotation is located. The number of rings at the central part of the pattern increases by increasing the exposure number. For example, for eighteen exposures with a rotation angle of $\varphi_i = 10°$ the number of rings formed is 4 and for 36 exposures with $\varphi_i = 5°$. the number of rings formed is 10. These results show that LIL can be used to fabricate diffractive and micro-optical elements, such as diffractive (Fresnel-) lenses. Fig. 7 shows a 3D simulated profile of concentric rings. The difference between radii of two adjacent rings is the same for all the rings. According to our simulations and data analysis the radii of the rings are only dependent on λ and θ. The difference

between the radii of two adjacent rings is $\Delta r = (\lambda/2)sin\theta$, which is in agreement with the interference patterns periodicity (Eq.10). Rings with minimum intensities are located exactly between rings with maximum intensities. Therefore, we can obtain ring radii if we know the radius of the first ring. We found that the radius of the first ring can be expressed by

$$r_0 \cong 0.61(\lambda/2\sin\theta) = 0.61P, \tag{11}$$

where P is pattern periodicity in single exposure (see Eq. 10). A simple mathematical approach shows that the radii of the rings can be obtained from

$$r_n \cong r_0 + (n-1)p = (n-0.39)P, \tag{12}$$

where n is an integer and starts from one.

In order to show how rings appear in multiple exposure-LIL, we wrote a simple computer program to generate several parallel lines such as those appearing in single exposure. Then the lines were rotated n=36 times around an axis (Fig. 8). It can be seen how the circular patterns form.

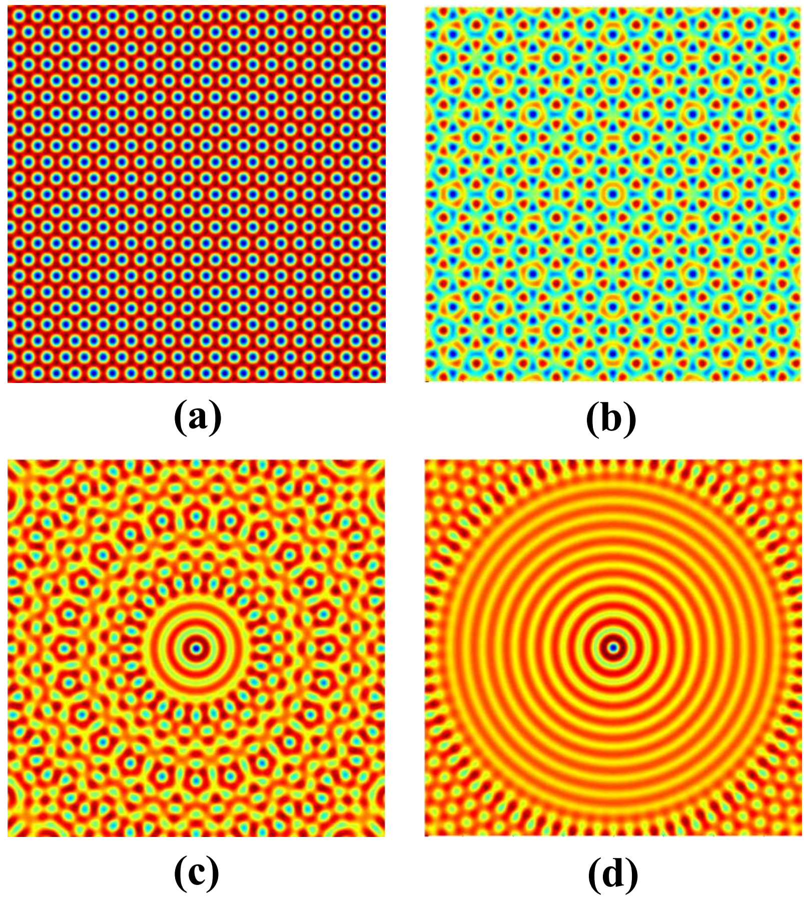

Fig. 6 Simulated interference pattern: a) n = 3, b) n = 4, c) n = 12, and d) n = 36. The exposure times of two successive rotations were equal.

.

Fig.7 3-D view of the simulated pattern in which $\lambda = 442nm$, $\varphi_i = 2°$ for 90 rotations

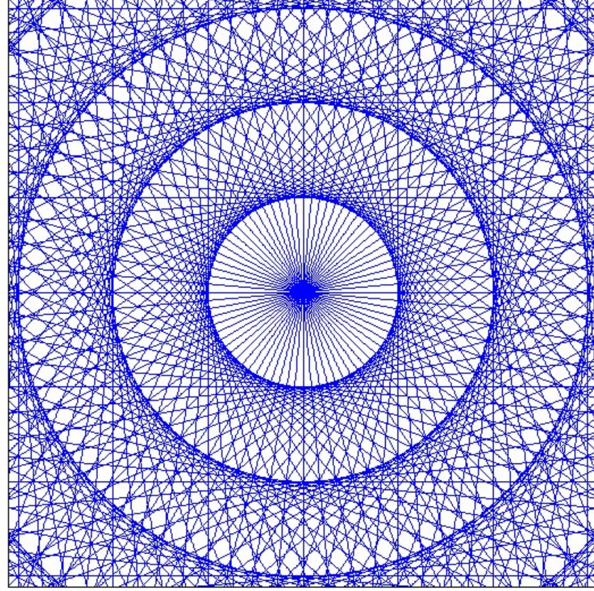

Fig.8. A pattern which is created by n=36 rotations of several parallel, equally spaced lines.

Figure 9 shows some of the resulting simulation patterns from multiple exposures with varying angles ϕ_i and exposure times t_i. The rotation angles of two successive exposures are not equal but the exposure times for two successive exposures are equal ($\phi_i \neq \phi_{i+1}$ and $t_i = t_{i+1}$). Fig. 10 shows a simulated pattern for n = 6. Rotation angles are all equal (30°), but exposure times are varied: $t_4 = t_1,\ t_5 = t_2 = 2t_1,\ t_6 = t_3 = 3t_1$

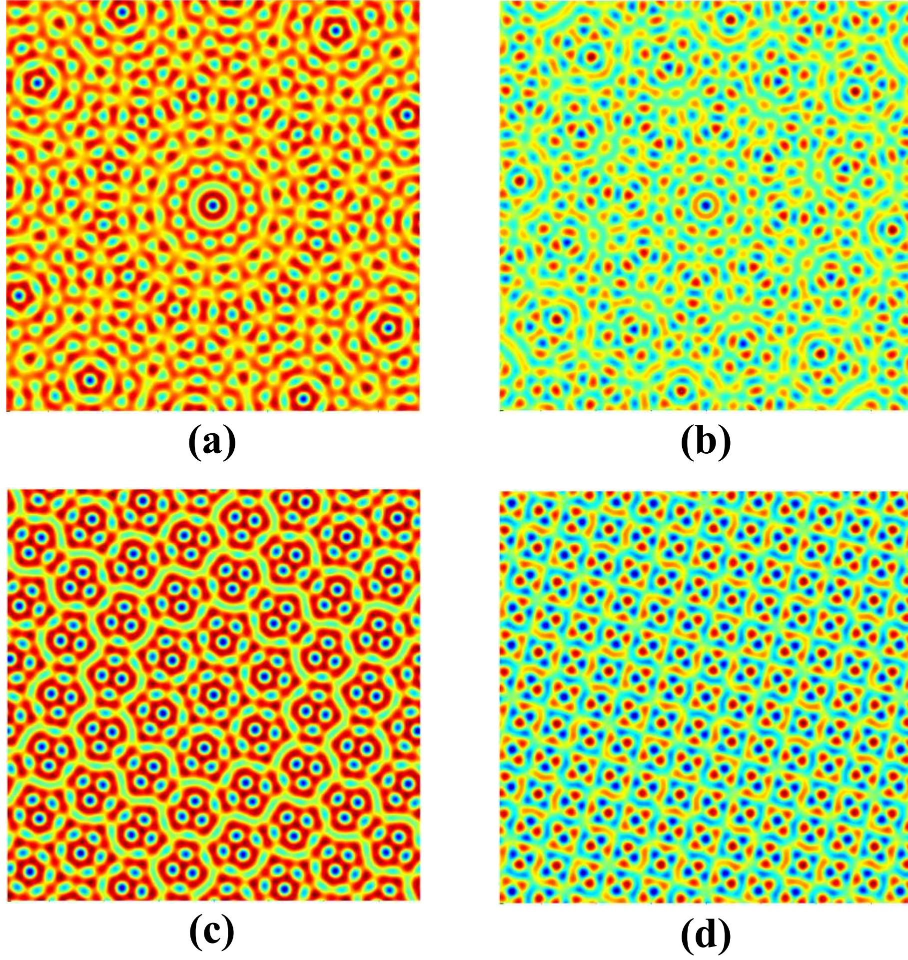

Fig. 9 Simulated pattern for multiple exposures. For two successive exposures $\mathrm{t_i} = \mathrm{t_{i+1}}$ but the rotation angles were (a) $\varphi_{2i-1} = 10^{\circ}$and $\varphi_{2i} = 20^{\circ}$ (b) $\varphi_{2i-1} = 15^{\circ}$ and $\varphi_{2i} = 30^{\circ}$ (c) $\varphi_{2i-1} = 20^{\circ}$ and $\varphi_{2i} = 40^{\circ}$ (d) $\varphi_{2i-1} = 30^{\circ}$ and $\varphi_{2i} = 60^{\circ} (i = 1, 2, \ldots)$

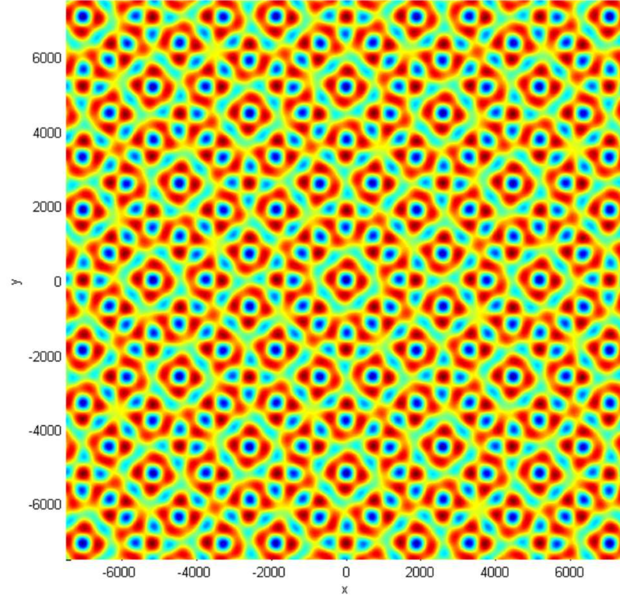

Fig.10 Simulated pattern for n = 6. Rotation angles were all equal 30° but exposure times were varied: $t_4 = t_1,\ t_5 = t_2 = 2t_1,\ t_6 = t_3 = 3t_1$

6 Conclusion

Single, double and multiple exposures in laser interference lithography were simulated. For single and double exposures samples were fabricated to ensure a proper functioning of the simulation tool. In addition a recipe was developed to fabricate photoresist nanofibers detaching from the silicon substrate surface. The simulation results are consistent with the experimental outputs. Simulations were carried out for multi-exposures and a variety of patterns obtained. The simulation results showed that LIL can be used to fabricate circular structures similar to Fresnel-lenses. These results show that LIL is not only able to produce 1D and 2D nanostructures but is able to fabricate nano- and micro- rings having applications in devices needing diffractive optical elements.

References

1. D. Wang et al., "Effects of polarization on four-beam laser interference lithograph," *Appl. Phys. Lett.* **102**(081903-081905 (2013).
2. I. B. Divliansky et al., "Fabrication of two-dimensional photonic crystals using interference lithography and electrodeposition of CdSe," *Appl. Phys. Lett.* **79**(3392-3394 (2001).
3. A. Hassanzadeh, and K. K. Wong, "Waveguide evanescent field fluorescence microscopy: waveguide mode scattering by non-uniform grating and defects in the wave guiding film," *Proc. SPIE* 73861-73868 (2009).
4. M. Zheng et al., "Magnetic nanodot arrays produced by direct laser interference lithograph," *Appl. Phys. Lett.* **79**(2606-2608 (2001).
5. J. Wanga, and H. Liang, "Interference lithography for metal nanopattern fabrication assisted by surface plasmon polaritons reflecting image," *J. Appl. Phys.* **113**(233101-233104 (2013).
6. D. W. Hamilton et al., "Migration of Periodontal Ligament Fibroblasts on Nanometric Topographical Patterns: Influence of Filopodia and Focal Adhesions on Contact Guidance," *Plosone* **5**(12), (2010).
7. H. P. Herzig, *Micro-Optics: Elements, Systems, and Applications*, Taylor & Francis, London (1997).
8. M. Switkes, T. M. Bloomstein, and M. Rothschild, "Patterning of sub-50 nm dense features with space-invariant 157 nm interference lithograph," *Appl. Phys. Lett.* **77**(3149-3151 (2000).
9. A. A. Letailleur et al., "High order symmetry interference lithography based nanoimprint," *J. Appl. Phys.* **109**(016103-016104 (2011).
10. J. H. Seo et al., "Large-Area Printed Broadband Membrane Reflectors by Laser IInterference Lithography," *IEEE Photonics journal* **5**(1), 2200106 (2013).

11. J. M. Cees, "Laser interference as a lithographic nanopatterning tool," *J. Microlith., Microfab., Microsyst.* **5**(1), 0110121-0110126 (2006).

12. X. Mai, "Simple versatile method for fabricating guided-wave gratings," *Appl. Opt.* **24**(19), 3155-3161 (1985).

13. A. Rodriguez et al., "Laser interference lithography for nanoscale structuring of materials: From laboratory to industry," *Microelectronic Engineering* **86**(937-940 (2009).

14. K. Petter et al., "Fabrication of large periodic arrays of AlGaAs microdisks by laser-interference lithography and selective etching," *Appl. Phys. Lett.* **81**(4), 592-594 (2002).

15. M. Campbell et al., "Fabrication of photonic crystals for the visible spectrum by holographic lithography," *Nature* **404**(53-56 (2000).

16. D. Mei et al., "Three-dimensional ordered patterns by light interference," *Opt. Lett.* **20**(5), 429-431 (1995).

17. J. H. Moon, J. Ford, and S. Yang, "Fabricating three-dimensional polymeric photonic structures by multi-beam interference lithography," *Polym. Adv. Technol.* **17**(83-93 (2006).

18. J. J. Cowan, and W. D. Slafer, "The Recording and Replication of Holographic Micropatterns for the Ordering of Photographic Emulsion Grains in Film Systems," *J. Imaging Sci.* **31**(100-107 (1987).

19. E. B. Kley, "Continuous profile writing by electron and optical lithography," *Microelectronic Engineering* **34**(261-298 (1997).

20. Q. Xie et al., "Fabrication of nanostructures with laser interference lithography," *Journal of Alloys and Compounds* **449**(261-264 (2008).

21. A. Fernandez et al., "Magnetic Force Microscopy of Single-Domain Cobalt Dots Patterned Using Interference Lithography," *IEEE Trans. Magn.* **32**(5), 4472-4474 (1996).

22. J. P. Spallas, A. M. Hawryluk, and D. R. Kania, "Field emitter array mask patterning using laser interference lithography," *J. Vac. Sci. Technol. B* **13**(5), 1973-1978 (1995).

23. I. Wathuthanthri, M. Weidong, and C. Choi, "Two degrees-of-freedom Lloyd-mirror interferometer for superior pattern coverage area," *optics letters* **36**(9), 1593-1595 (2011).

24. A. Ritucci et al., "Interference lithography by a soft x-ray laser beam: Nanopatterning on photoresists," *J. Appl. Phys.* **102**(0343131-0343134 (2007).

25. L. Qian et al., "Tilted and axis-shift Lloyd's mirror system for recording low-densityand large-area holographic grating," *optik* **125**(1287– 1291 (2014).

26. E. Ertorer et al., "Large Area Periodic, Systematically Changing, Multi-Shape Nanostructures by Laser Interference Lithography and Cell Response to these Topographies," *Biomedical Optics* **18**(3), 035002 (2013).

27. K. Bao et al., "Improvement of light extraction from GaN-based thin-film light-emitting diodes by patterning undoped GaN using modified laser lift-off," *Appl. Phys. Lett.* **92**(141103-141104 (2008).

28. L. Cerdán et al., "Laser emission from mirrorless waveguides based on photosensitized polymers incorporating POSS," *Opt. Express* **18**(10), 10247-10256 (2010).

29. K. Wang, "Light localization in photonic band gaps of quasiperiodic dielectric structures," *Phys. Rev. B* **82**(045119 (2010).

30. W. Zhou et al., "Enhanced efficiency of light emitting diodes with a nano-patterned gallium nitride surface realized by soft UV nanoimprint lithography," *Nanotechnology* **21**(205304 (2010).